

Wide viewing angle realization for sampled hologram by collecting high-order diffraction beams

Byung Gyu Chae

Basic Research Laboratory, Electronics and Telecommunications Research Institute, 218

Gajeong-ro, Daejeon 305-700, South Korea

Abstract

We analyze the change in viewing angle of the holographic image for the on-axis hologram by varying an incidence angle of a plane wave. The tilted plane wave plays a role in a modulated carrier similar to a carrier signal of the off-axis holography, which makes the diffractive wave propagating to new optical axis direction. In the Fresnel hologram, new viewing zone of the reconstruction image is formed, but its image shape is deformed along new viewing direction. The Fourier hologram enables to retrieve three-dimensional image with other perspective by a tilted plane wave. The sampled hologram with pixel structure generates high-order diffraction beams propagating to various directions. Collection of diffracted beams to a definite image spot effectively increases a viewing zone angle of the reconstruction image. We conduct the numerical analysis for the sampled hologram showing high-order diffraction beams with various viewing zones.

OCIS codes: (090.2870) Holographic display; (090.1995) Digital holography;
(090.1970) Diffractive optics

1. Introduction

The hologram implies three-dimensional information with phase and amplitude of the propagating wave [1,2]. This makes it possible to retrieve the wavefront of original propagating wave by illuminating the hologram with reconstructing wave. However, in digital holography, the holography has difficulty in the recording and reconstructing processes of the hologram image because of high spatial frequency of the fringe pattern [3-5]. The hologram is the interference fringe of the recording wave and the object wave, and therefore, for retrieving the hologram image with sufficient viewing angle the spatial frequency gets to the extent of the wavelength of the light field.

In holographic display, the hologram is sampled with sampling frequency of the device with pixel structure to avoid aliasing effects [6,7]. Present modulator encoding hologram fringe has much lower resolution than the required specification. Now, the limitation of the spatial frequency due to the device performance obstructs widening view angle of the hologram image, although the holographic display can reconstruct the image to the display size. For the realization of holographic display, solving the problem of widening viewing angle is essential.

Current researches for improving the viewing zone have been carried out through the spatial multiplexing of the spatial light modulators [8-10]. Curved array of the devices effectively enhances the viewing angle of the reconstructed image, where from the stereogram representing each view, the large space-bandwidth product is still required. Since only the high-definition resolution of the digital image is sufficient, the massive hologram data for displaying holographic high-definition image is considered to be absurd. This also hinders the process of the digitized hologram data.

In this research, we note that in principle, even the hologram with small space bandwidth has entire information of the object, and thus trying to find how to enlarge the viewing zone of the reconstructed image optically. First, for the Fresnel and Fourier holograms we investigate the possibility of the viewing angle change by varying an incidence angle of the

illuminating plane wave. The plane wave illuminating the hologram in other direction than that of the recording process generates diffracted beams emanating to the shifted position of the reconstructed image, which can make the viewing zone with another perspective of the image. Next, in the sampled hologram with pixel structure the method of extending the viewing zone angle by collecting high-order diffracted beams is proposed. Finally, we carry out the numerical analysis for the sampled hologram showing high-order diffraction beams with various viewing zones.

2. Viewing angle analysis of hologram image

A. Reconstruction process by a tilted plane wave

The reconstruction process of the objective wave in the on-axis hologram illuminating by a tilted plane wave, $\exp(jk_0x \sin \theta)$ is expressed as the product of a hologram component, $a(x, y) \exp[j\phi(x, y)]$ and the illuminating wave.

$$a(x, y) \exp[j\phi(x, y)] \exp(jk_0x \sin \theta) \quad (1)$$

When the plane wave with unit amplitude is used in recording the on-axis hologram, $a(x, y)$ and $\phi(x, y)$ are real amplitude and phase of the object wave, respectively. Equation (1) can be rewritten as another form.

$$a(x, y) \exp \{j[\phi(x, y) + k_0x \sin \theta]\} \quad (2)$$

This is a kind of the reconstruction form for the off-axis hologram made by the recording plane wave, $\exp(jk_0x \sin \theta)$, where the coaxial reconstruction wave is assumed. Equation (2) can be also rewritten by varying together incidence angle values of the recording and reconstructing plane waves in the off-axis hologram. In a view of the carrier frequency holography, the on-axis hologram fringe is unique because it has a constant form as the modulating signal irrespective of the spatial carrier. Therefore, in two cases of the on-axis holography by an inclined plane wave and the off-axis holography, there is only the variation of the carrier frequency.

$$f_c = \frac{\sin \theta}{\lambda} \quad (3)$$

Figure 1 depicts the reconstruction by illuminating the on-axis hologram with the plane wave at an incidence angle, θ . Here, we notice only the real image from the complex amplitude modulation in order to clarify our analysis. The viewing angle of the image by the coaxial plane wave is determined by means of the spatial frequency of the fringe pattern. Since the local spatial frequency is given by $\frac{x}{\lambda z_0} \approx \frac{\sin \omega}{\lambda}$, the viewing angle, Ω is double the size of ω . The higher spatial frequency leads the wider viewing angle of the image. In the tilted plane wave, since the exponential term of a carrier frequency generates the deflected beam of the retrieved image, the viewing zone of the object image changes to new Ω_{NEW} region in Fig. 1.

We find that the tilted plane wave plays a role in a modulated carrier similar to a carrier signal of the off-axis holography, which makes the diffractive wave propagating to new optical axis direction. In the sampled hologram, the viewing zone of the reconstructed image has a limitation because it has the bandlimit signal to the Nyquist frequency to avoid the aliasing effect [11]. But, the viewing zone variation of the object image by a tilted plane wave is irrespective of the aliasing in principle. This case is different from the aliasing arising in sampling the modulated carrier signal to the hologram. Here, the modulating hologram signal of the object is already recorded in the sampled hologram, and only the inclined reconstruction wave related to the carrier signal is illuminated. Thus, by controlling the incidence angle of the reconstruction wave for the on-axis sampled hologram, we can get the reconstruction effect of the off-axis holography making a new viewing zone.

B. Hologram image deformation by a tilted plane wave

Let us investigate the change in the reconstructed image of the hologram transparency, $g(x, y)$ by a tilted plane wave. The complex field of the image in the Fresnel propagation is developed as the convolution of the input field, $\exp[jk_0(x \sin \theta + y \sin \varphi)]g(x, y)$ and the

spatial impulse response, $h(x, y; z_0) = \frac{1}{j\lambda z_0} \exp(-jk_0 z_0) \exp\left[-j\frac{k_0}{2z_0}(x^2 + y^2)\right]$.

$$U(x, y; z_0) = \frac{e^{jk_0 z_0}}{j\lambda z_0} \exp\left[-j\frac{k_0}{2z_0}(x^2 + y^2)\right] \iint \exp[jk_0(x' \sin \theta + y' \sin \varphi)] g(x', y') \\ \times \exp\left[-j\frac{k_0}{2z_0}(x'^2 + y'^2)\right] \exp\left[j\frac{2\pi}{\lambda z_0}(xx' + yy')\right] dx' dy' \quad (4)$$

The integral part can be calculated from the convolution operation of two Fourier transforms of the product term of the hologram and the plane wave and the quadratic phase term.

$$G\left[\frac{1}{\lambda z_0}(x + z_0 \sin \theta, y + z_0 \sin \varphi)\right] * H(f_X, f_Y) \quad (5)$$

where $H(f_X, f_Y)$ is the transfer function in the Fresnel diffraction.

$$\iint G(f'_X + f_{Xc}, f'_Y + f_{Yc}) H(f_X - f'_X, f_Y - f'_Y) df'_X df'_Y \quad (6)$$

By inserting Eq. (6) into Eq. (4), above equation is the angular spectrum representation of the field propagation in the Fresnel diffraction. If we substitute the variables, $f'_X + f_{Xc}$ by f''_X and $f'_Y + f_{Yc}$ by f''_Y and rearrange the equation, it becomes the expression for the complex field of the object shifted to the transversal axis.

$$U(x + z_0 \sin \theta, y + z_0 \sin \varphi; z_0) \quad (7)$$

The tilted plane wave causes the image reconstructed at the shifted position to the transversal axis. This analysis is applicable to the arbitrary incidence angle of the tilted plane wave, because the diffraction beam to retrieve an image can be regarded as the paraxial propagation along the new diffraction optical-axis. Figure 2(a) shows two-dimensional plane image vertical to optical axis retrieved at the shifted position by an inclined plane wave to x -axis. We find that in a plane object, new viewing angle of the image is generated, because only the lateral position of the reconstructed image is shifted without distortion of the object shape.

However, in a three-dimensional object, a change of an image shape occurs. The three-dimensional object image can be calculated at various z values.

$$\sum_l U(x + z_l \sin \theta, y + z_l \sin \varphi; z_l) \quad (8)$$

The amount of shifted value to transversal axis depends on the z value, which invokes an image deformation along the depth direction. The retrieved image of the hologram composed of the point sources in x - z plane is illustrated in Fig. 2(b). The point image is obtained from the simple convolution expression about one-point hologram [12].

$$\begin{aligned} & \exp(jk_0 x \sin \theta) \exp \left[j \frac{k_0}{2z_0} (x^2 + y^2) \right] * h(x, y; z_0) \\ \sim & \iint \exp \left\{ j \frac{k_0}{z_0} [(x + z_0 \sin \theta)x' + yy'] \right\} dx' dy' \sim \delta(x + z_0 \sin \theta, y) \end{aligned} \quad (9)$$

For convenience, the coefficient of each term shall drop. The first line of above equation is also presented as the reconstruction of the off-axis hologram as like $\exp \left\{ j \left[-\frac{k_0}{2z_0} (x^2 + y^2) + k_0 x \sin \theta \right] \right\} * h(x, y; z_0)$. The real image appears as the delta function. If $\sin \theta$ is written by $\frac{x_p}{z_0}$, the point image moves to x_p amount at x axis. Here, deflection beam angle does not exactly coincide with an incidence beam angle. Four real images are reconstructed at following locations, where the interval between two points in the axial direction is put to be c .

$$\begin{aligned} & \delta \left(x - \frac{c}{2} + x_{p1}, y; z_0 - \frac{c}{2} \right) + \delta \left(x + \frac{c}{2} + x_{p1}, y; z_0 - \frac{c}{2} \right) \\ & + \delta \left(x - \frac{c}{2} + x_{p2}, y; z_0 + \frac{c}{2} \right) + \delta \left(x + \frac{c}{2} + x_{p2}, y; z_0 + \frac{c}{2} \right) \end{aligned} \quad (10)$$

where x_{p1} and x_{p2} are the values, $(z_0 - c/2) \sin \theta$ and $(z_0 + c/2) \sin \theta$.

As shown in Fig. 2(b), shearing transformation arises along x -axis. The image deformation by a tilted reconstruction plane wave, $\exp[jk_0(x \sin \theta + y \sin \varphi)]$ is described in terms of Affine transformation.

$$\begin{pmatrix} x' \\ y' \end{pmatrix} = \begin{pmatrix} 1 & m \\ n & 1 \end{pmatrix} \begin{pmatrix} x \\ y \end{pmatrix} + \begin{pmatrix} z \sin \theta \\ z \sin \varphi \end{pmatrix} \quad (11)$$

We find that the reconstruction plane wave incident on at a different angle from that of the recording process definitely induces the deformation of a retrieved image, which holds for both on-axis and off-axis holograms. Although the plane object image makes a new

viewing zone in terms of an inclined plane wave, three-dimensional image does not form new entire view in the Fresnel hologram. That is, at a viewing direction observer sees the projection scene of reconstruction image by coaxial plane wave with respect to vertical plane of deflection axis, but deformed image shape.

C. Viewing angle change for the Fourier hologram image

Figure 3 illustrates the reconstruction process for the Fourier hologram by a tilted plane wave. The hologram plane is placed in the front focal plane of the convex lens of focal length, f . The field distribution of the image in the vicinity of the back focal plane, d is obtained from below equation [13,14].

$$U(x, y; \Delta z) = \frac{1}{j\lambda f} \iint \exp[jk_0(x' \sin \theta + y' \sin \varphi)] g(x', y') \times \exp \left(-\frac{j2\pi}{\lambda} \left[\frac{(x'^2 + y'^2)\Delta z}{2f^2} - \frac{(xx' + yy')}{f} \right] \right) dx' dy' \quad (12)$$

where $\Delta z = f - d$ indicates the image depth distribution. From the similar interpretation of Eqs. (4)-(7) in the Fresnel hologram, we can get the expression for the complex field of the object image shifted to the transversal axis.

$$U(x + f \sin \theta, y + f \sin \varphi; \Delta z) \quad (13)$$

Here, the shift quantity to the transversal axis has a constant value as $f \sin \theta$ or $f \sin \varphi$ irrespective of the image depth, and thus, as different from the Fresnel hologram, the image deformation does not occur along the viewing direction.

The tilted plane wave does not change the shape of the reconstructed image and only moves the image to lateral position, as depicted in Fig. 3. Therefore, the inclined plane wave can vary effectively the viewing angle of some object image reconstructed optically as a function of the incidence angle in the Fourier hologram. We clearly confirm that the perspective of the object image changes according to the propagation direction of diffracted beams. Considering the virtual image formation with opposite view of the real image, it

is apparent that even the hologram with extremely low spatial-frequency shall retrieve the whole view of the object image optically in a transparent object. This is possible because the hologram has entire information of three-dimensional object.

We assume that the viewing angle of the object is widened by collecting above diffraction beams propagating to various directions. Figure 4 is a typical example of obtaining the wide viewing angle of the image by varying an incidence angle of the plane wave. Here, the deflection device should sufficiently collect diffracted beams to a definite image spot. If the device is far apart from the hologram plane, it will be a single type with respect to diffracted beams in Fig. 4. But if not, the device has a separate specification according to the beams. And for the large incidence angle, the correction of the optical path length is required as an amount, $2d_0(\frac{1}{\cos\theta} - 1)$.

3. Expansion of viewing angle in sampled hologram

The sampled hologram in holographic display generates high-order diffracted beams due to pixel structure. The diffracted beams propagate in the direction at an angle with respect to the optical z -axis. We investigate the possibility of widening viewing angle by collecting diffracted beams to a definite image spot. Figure 5 illustrates the schematic diagram of forming the holographic image on the basis of our deduction. The optical element between the hologram component plane involving the Fourier lens and the image plane plays a role in collecting diffracted beams. That is, this device deflects diffracted beams to the image spot.

We assume the sampled Fourier hologram, $g_s(\xi, \eta)$ by rectangular pixels in Fig. 6, which has the pixel interval p_ξ and the pixel size Δp_ξ in the ξ -direction, and p_η , Δp_η in the η -direction.

$$g_s(\xi, \eta) = \sum_{n_\xi=-\infty}^{\infty} \sum_{n_\eta=-\infty}^{\infty} \left[g(n_\xi p_\xi, n_\eta p_\eta) \text{rect} \left(\frac{\xi - n_\xi p_\xi}{\Delta p_\xi}, \frac{\eta - n_\eta p_\eta}{\Delta p_\eta} \right) \right] \quad (14)$$

where $\text{rect}()$ is a rectangular function. The amplitude distribution in front of the optical

element is represented by the convolution notation.

$$U_p(x, y) = \left([g_s(x, y) * h(x, y; f)] \exp \left[j \frac{k}{2f} (x^2 + y^2) \right] \right) * h(x, y; z_1) \quad (15)$$

where z_1 is the distance between the hologram component plane and the deflection plane. We consider the normally incident plane wave with unit amplitude. The complex field in the image plane is obtained using above equations.

$$\begin{aligned} U(u, v) &= [U_p(u, v) t_p(u, v)] * h(u, v; z_2) \\ &= \frac{j}{\lambda z_2} \exp \left[-j \frac{k}{2z_2} (u^2 + v^2) \right] \iint U_p(x, y) \exp \left[-j \frac{k}{2z_2} (x^2 + y^2) \right] \exp \left[j \frac{2\pi}{\lambda z_2} (xu + yv) \right] dx dy \\ &\quad * \iint t_p(x, y) \exp \left[j \frac{2\pi}{\lambda z_2} (xu + yv) \right] dx dy \quad (16) \end{aligned}$$

The $t_p(x, y)$ is the amplitude transmittance of the deflection element, and the z_2 is the distance between the deflection plane and the image plane.

The field distribution, $U_p(x, y)$ is simplified to the Fourier spectrum of the sampled hologram in case of the z_1 equal to the focal length of the lens [13]. At first, for analysis of the property of diffraction beams we evaluate the Fourier transform of Eq. (14).

$$\begin{aligned} &\iint g_s(\xi, \eta) \exp \left[j 2\pi \left(\frac{x\xi}{\lambda z_1} + \frac{y\eta}{\lambda z_1} \right) \right] d\xi d\eta = \\ \Delta p_\xi \Delta p_\eta \text{sinc} \left(\frac{\pi x \Delta p_\xi}{\lambda z_1} \right) \text{sinc} \left(\frac{\pi y \Delta p_\eta}{\lambda z_1} \right) &\sum_{n_\xi=-\infty}^{\infty} \sum_{n_\eta=-\infty}^{\infty} \left[g(n_\xi p_\xi, n_\eta p_\eta) \exp \left\{ j \frac{2\pi}{\lambda z_1} (n_\xi p_\xi x + n_\eta p_\eta y) \right\} \right] \quad (17) \end{aligned}$$

If the $g(n_\xi p_\xi, n_\eta p_\eta)$ is a constant number, the summation part becomes the Dirac comb function, which makes just the Fraunhofer diffraction of the rectangular pixel array. Inserting the value of the sampled hologram, this term turns into the Fourier spectrum. The summation term is rewritten as the Fourier transform through the Poisson summation formula.

$$\sum_{\alpha=-\infty}^{\infty} \sum_{\beta=-\infty}^{\infty} G \left[\frac{1}{\lambda z_1} \left(x - \frac{\lambda z_1}{p_\xi} \alpha \right), \frac{1}{\lambda z_1} \left(y - \frac{\lambda z_1}{p_\eta} \beta \right) \right] \quad (18)$$

From this, Eq. (17) describes the modulation of the periodic Fourier spectrum by the envelope of the sinc function along the x - and y -axis. We briefly depict the modulated curve by the sinc function in Fig. 7. If the pixel interval $p_{\xi, \eta}$ is put to be approximately equal to the

pixel size $\Delta p_{\xi,\eta}$, the zeroth-order diffraction beam well implies the zeroth-order spectrum image. But the high-order images are centered at the minimum region of the envelope because the main lobe of the sinc function has twice the width of other beams. This can be overcome by the phase-shift technology, which appropriately controls the position of the reconstructed image to the transverse axis.

The complex field of the object in the deflection plane is distributed within each diffracted beam at the interval of $\frac{\lambda z}{p}$ or $\frac{\lambda z}{\Delta p}$. Equation (18) can be expressed as another form as follows.

$$\begin{aligned} & \sum_{\alpha=-\infty}^{\infty} \sum_{\beta=-\infty}^{\infty} \mathcal{F} \left\{ g(\xi, \eta) \exp \left[j2\pi \left(\frac{\alpha}{p_{\xi}} \xi + \frac{\beta}{p_{\eta}} \eta \right) \right] \right\} \\ = & \sum_{\alpha=-\infty}^{\infty} \sum_{\beta=-\infty}^{\infty} \mathcal{F} \{ g(\xi, \eta) \exp[jk(\xi \sin \theta_{\alpha} + \eta \sin \theta_{\beta})] \} \end{aligned} \quad (19)$$

where the diffraction relation, $p_{\xi} \sin \theta_{\alpha} = \alpha \lambda$ and $p_{\eta} \sin \theta_{\beta} = \beta \lambda$, are applied. As stated in Section 2, above equation presents the diffraction of the $g(\xi, \eta)$ object with the spatial frequency $\frac{(x,y)}{\lambda z}$ by illuminating with the inclined plane wave at an incidence angle $\theta_{\alpha,\beta}$. Therefore, we find that high-order diffraction beams create the new viewing zone with different perspective of the object.

Figure 8 is a system for collecting high-order diffracted beams to enlarge viewing angle. For convenience, only the first-order beam along the x -axis is displayed. The prism as an optical deflection device is used to bend diffracted waves to the same place of the image plane. The phase transformation of the deflection device is generally written by $\exp(-jkx \sin \theta)$. High-order diffraction beams should be deflected at the different angle according to the diffraction order. The amplitude transmission of this device has a separated value distributed with the space, Δw of the beams.

$$\begin{aligned} t_p(x, y) = & \sum_{n_x} \exp \left[-jk \sin \theta_{n_x} \left\{ x + w_x(n_x + \frac{1}{2}) \right\} \right] \text{rect} \left(\frac{x - w_x(n_x + 1/2)}{\Delta w_x} \right) \\ & + \sum_{n_y} \exp \left[-jk \sin \theta_{n_y} \left\{ y + w_y(n_y + \frac{1}{2}) \right\} \right] \text{rect} \left(\frac{y - w_y(n_y + 1/2)}{\Delta w_y} \right) \end{aligned} \quad (20)$$

The $w_{x,y}$ is the shifted value equal to the beam space. Figure 9(a) exhibits the design of the deflection elements.

From the second term of the convolution in Eq. (16), we evaluate the Fourier transform of the amplitude distribution of the deflection device.

$$\begin{aligned} & \sum_{n_x} \left[\delta(u + z_2 \sin \theta_{n_x}) * \left\{ \text{sinc}\left(\frac{\pi u \Delta w_x}{\lambda z_2}\right) \exp \left[j \frac{2\pi u w_x}{\lambda z_2} \left(n_x + \frac{1}{2} \right) \right] \right\} \right] \\ & + \sum_{n_y} \left[\delta(v + z_2 \sin \theta_{n_y}) * \left\{ \text{sinc}\left(\frac{\pi v \Delta w_y}{\lambda z_2}\right) \exp \left[j \frac{2\pi v w_y}{\lambda z_2} \left(n_y + \frac{1}{2} \right) \right] \right\} \right] \end{aligned} \quad (21)$$

where the constant coefficient is omitted. In real system, since the space Δw of the diffraction beam in the deflection plane is very large, the sinc function can be regarded as the delta function. Furthermore, considering the spatial distribution of deflection devices with an interval of w value, the function together with exponential term is expressed as like $\delta(u - w_x(n_x + 1/2))$. Equation (21) is reduced to be the following delta function.

$$\sum_{n_x} \delta \left(u + z_2 \sin \theta_{n_x} - w_x \left(n_x + \frac{1}{2} \right) \right) + \sum_{n_y} \delta \left(v + z_2 \sin \theta_{n_y} - w_y \left(n_y + \frac{1}{2} \right) \right) \quad (22)$$

The first term of the convolution in Eq. (16) is also rewritten as $U_p(u, v) * h(u, v; z_2)$, where similar deduction in Section 2 is applied to obtaining the complex field, $U_i(u, v)$ in the image plane. From this, the wave field distribution in the image plane can be interpreted by simplified convolution expression as below.

$$\begin{aligned} U(u, v) & \cong \sum_{\alpha=-\infty}^{\infty} \sum_{\beta=-\infty}^{\infty} U_i \left(u - \frac{\lambda z_2}{p_\xi} \alpha, v - \frac{\lambda z_2}{p_\eta} \beta \right) \\ & * \left\{ \sum_{n_x} \delta \left(u + z_2 \sin \theta_{n_x} - w_x \left(n_x + \frac{1}{2} \right) \right) + \sum_{n_y} \delta \left(v + z_2 \sin \theta_{n_y} - w_y \left(n_y + \frac{1}{2} \right) \right) \right\} \end{aligned} \quad (23)$$

In our system in Fig. 8, each deflection element operates only the diffraction beam with corresponding order, and thus the convolution is carried out between two terms with same order. If we select an adequate deflection angle corresponding to the diffraction angle of the beam, diffraction beams can be collected at a particular image spot. In case of equal distance of z_1 and z_2 values, the deflection angle, $\sin \theta_{n_x, n_y}$ becomes double compared to the diffraction angle, $\sin \theta_{\alpha, \beta}$, as depicted in Fig. 9(b). The transverse location component compensates the shift quantity of the delta function to match with two terms of the convolution operation. We can finally obtain all diffracted beams gathering in the zeroth-order region in the image plane.

$$\sum_{\alpha,\beta} U_{\alpha,\beta}(u', v') \quad (24)$$

Here, the deflection operation is exerted at the shifted location of the x - y deflection plane in Fig. 9(b). Therefore, in a view of the deflection plane, above equation implies the reconstruction by diffracted beams at a different angle.

$$\sum_{\alpha=-\infty}^{\infty} \sum_{\beta=-\infty}^{\infty} \mathcal{F}\{u(x, y) \exp[jk(x \sin \theta_{\alpha} + y \sin \theta_{\beta})]\} \quad (25)$$

The wide viewing angle of the holographic image is realized only by collecting high-order diffraction beams with different perspectives.

4. Numerical analysis of the sampled hologram

The outline of the sampled hologram for the numerical analysis is illustrated in Fig. 10. The hologram is sampled in the rectangular pixel array, where the size of the pixel array is 200×200 and the interval of the pixels, p is set to be $4 \mu\text{m}$. Based on the rectangular function in Eq. (14), each pixel is divided into several subpixels, which makes it possible to display high-order images in the entire area of the reconstruction picture. Here, the number of subpixels is put to be ten, and then, the total resolution of the device encoding the sampled hologram becomes to be 2000×2000 .

We prepared the Fresnel hologram with 200×200 resolution about the object of ‘HOLO’ letter in Fig. 11. The hologram was synthesized at $z = 0.2 \text{ m}$ apart from the object plane by using the recording plane wave with wavelength of 632.8 nm , where the border between pixels is one subpixel with $0.4 \mu\text{m}$ thickness and the pixel size, Δp becomes $3.6 \mu\text{m}$. Each hologram data is recorded in the 200×200 corresponding pixel array. That is, the hologram data within a single pixel of the device has the same value.

Figure 12 is the numerically reconstructed image by using above sampled hologram. For convenience, the complex modulation is considered. We find that high-order reconstructed images generate, whose intensity varies according to the envelope of the sinc function. The ten high-order images up to fifth order are displayed in figure. The lower graph of Fig. 12(a)

shows the central cross-section spectrum along the x -axis. As discussed in Fig. 7, there is a misalignment between high-order images and the envelope of the sinc function. Figure 12(b) is the reconstructed image for the hologram made by adding the phase-shift component. The zeroth order image is placed in the half main lobe of sinc function, and the mismatch of high-order images is mostly improved. Here, half spatial bandwidth of the zeroth order diffraction is available. The board portion between pixels also causes the mismatch of the images. The envelope of the sinc function and the image spectrum are placed with period of $\frac{\lambda z}{\Delta p}$ and $\frac{\lambda z}{p}$, respectively. The ratio of the pixel size, Δp to the pixel interval, p determines the number of the image in the one lobe of the sinc function. We confirmed that the number of the image increases with decreasing the ratio. In above pixel structure, since the ratio is 90%, there appears the mismatch of up to 10% per one order image. For well matching, the pixel size should be designed very close to the pixel interval.

In Fig. 12, high-order images have the same plane picture, which is consistent with interpretation of Section 2. That is, diffraction beams only move the images to the transverse axis without their deformation. In order to investigate the object view of high-order images, the object image should be numerically reconstructed in the direction of the optical diffraction axis. Figure 13(a) illustrates the coordinate transformation to the optical diffraction direction. The each order image is reconstructed at the new x_o - y_o coordinate. The images reconstructed in the several diffraction directions are appeared in Figure 13(b). The tilted angle is determined by diffraction order, where for visualization, large diffraction angle was adopted. The numerical simulation is carried out for each diffraction order independently, where the interpolation operation is applied [15-17]. The reconstructed image is shrunk in the x_o -axis direction. The higher diffraction angle leads to the larger image contraction. The contraction of the images is natural because the reconstructed images can be regarded as the projection images to the tilted plane. Therefore, we find that especially in the Fourier hologram the object view varies according to the diffraction order, as depicted in Fig. 3. The variation of the viewing angle shall be clarified by the numerical simulation of three-dimensional object.

Finally, we can extend the viewing zone angle of the reconstructed image by collecting diffraction beams to the main lobe of the sinc function. For this method, all of diffraction beams should have the same intensity to form the uniformly extended viewing-zone. The optical attenuator is one of methods for adjusting each beam intensity and correcting the optical path length. Furthermore, the spectrum intensity of a particular order can be arbitrarily controlled by the design of the diffracting grating. Therefore, the realization of this holographic display depends on the design of the pixel structure sampling the hologram data.

5. Conclusion

The illuminating plane wave to the Fresnel hologram at a different angle from the recording process leads to the formation of new viewing zone accompanied by the image deformation along viewing direction. The Fourier hologram makes it possible to retrieve three-dimensional image with other perspective by a tilted plane wave. In the sampled hologram with pixel structure, the viewing zone angle of the reconstructed image is effectively increased only by collecting high-order diffraction beams with different viewing direction. The design of the pixel structure creating high-order diffraction beams uniformly distributed is important for this holographic display. Further study for making various types of diffraction beams is required. This becomes one of the methods for overcoming the low spatial frequency making the narrow viewing angle.

REFERENCES

1. D. Gabor, “A new microscopic principle,” *Nature* **161**, 777-778 (1948).
2. E. N. Leith and J. Upatnieks, “Reconstructed wavefronts and communication theory,” *J. Opt. Soc. Am.* **52**, 1123-1130 (1962).
3. A. W. Lohmann and D. P. Paris, “Binary Fraunhofer holograms generated by computer,” *Appl. Opt.* **6**, 1739-1748 (1967).
4. P. St. Hilaire, S. A. Benton, M. E. Lucente, M. L. Jepsen, J. Kollin, H. Yoshikawa, and J. Underkoffler, “Electronic display system for computational holography,” *Proc. SPIE* **1212**, 174-182 (1990).
5. T. Yatagai, “Stereoscopic approach to 3-D display using computer generated holograms,” *Appl. Opt.* **15**, 2722-2729 (1976).
6. Y. Takaki and J. Nakamura, “Zone plate method for electronic holographic display using resolution redistribution technique,” *Opt. Express* **19**(15), 14707-14719 (2011).
7. T. Senoh, T. Mishina, K. Yamamoto, R. Oi, and T. Kurita, “Viewing-zone-angle-expanded color electronic holography system using ultra-high-definition liquid crystal displays with undesirable light elimination,” *J. Display Technol.* **7**(7), 382-390 (2011).
8. J. Hahn, H. Kim, Y. Lim, G. Park, and B. Lee, “Wide viewing angle dynamic holographic stereogram with a curved array of spatial light modulators,” *Opt. Express* **16**(16), 12372-12386 (2008).
9. F. Yaras, H. Kang, and L. Onural, “Circular holographic video display system,” *Opt. Express* **19**(10), 9147-9156 (2011).
10. G. Finke, T. Kozacki, and M. Kujawinska, “Wide viewing angle holographic display with multi spatial light modulator array,” *Proc. SPIE* **7723**, 77230A-8 (2010).
11. T. Mishina, M. Okui, and F. Okano, “Viewing-zone enlargement method for sampled

- hologram that uses high-order diffraction,” *Appl. Opt.* **41**, 1489-1499 (2002).
12. T. C. Poon, M. Wu, K. Shinoda, and Y. Suzuki, “Optical scanning holography,” *Proc. IEEE* **84**, 753-764 (1996).
 13. J. W. Goodman, “Introduction to Fourier optics,” 2nd ed. McGraw-Hill, 1996.
 14. H. Kim, J. Hahn and B. Lee, ”Mathematical modeling of triangle-mesh-modeled three-dimensional surface objects for digital holography,” *Appl. Opt.* **47**, D117-D127 (2008).
 15. D. Leseberg and C. Frere, “Computer-generated holograms of 3D objects composed of tilted planar segments,” *Appl. Opt.* **27**, 3020-3024 (1988).
 16. L. Yu, Y. An, and L. Cai, “Numerical reconstruction of digital holograms with variable viewing angles,” *Opt. Express* **10**, 1250-1257 (2002).
 17. K. Matsushima, H. Schimmel, and F. Wyrowski, ”Fast calculation method for optical diffraction on tilted planes by use of the angular spectrum of plane waves,” *J. Opt. Soc. Am. A* **20**, 1755-1762 (2003).

FIGURES

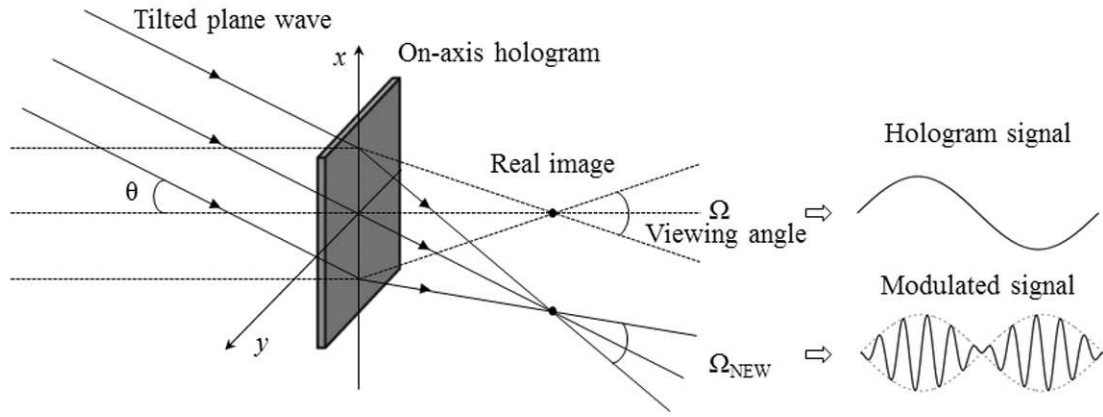


Fig. 1. The reconstruction process of the on-axis hologram by a coaxial plane wave and a tilted plane wave.

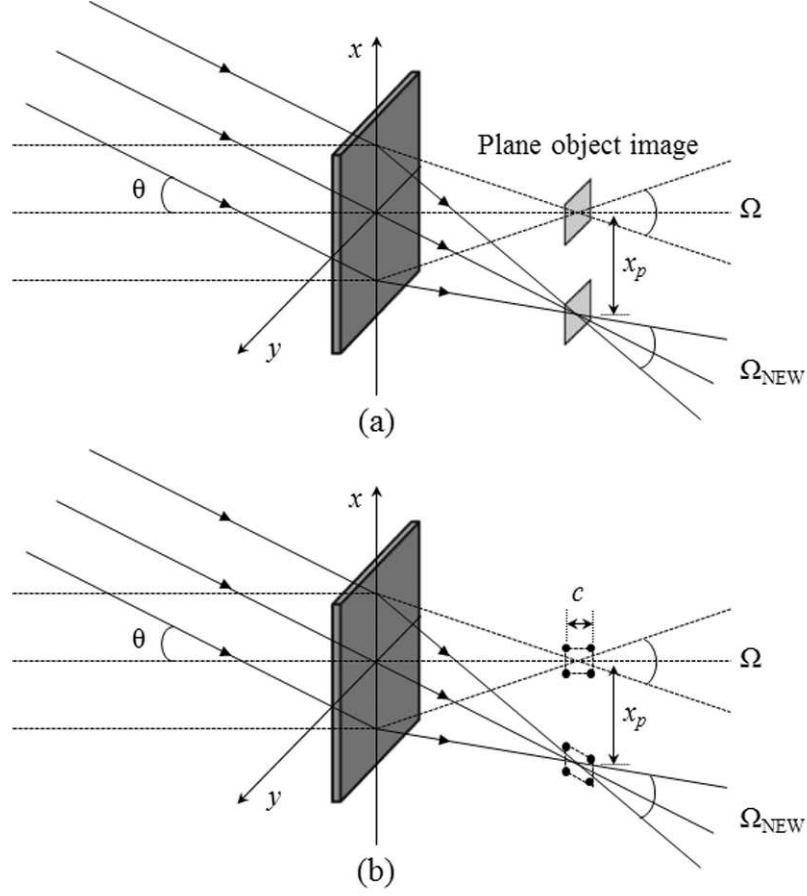


Fig. 2. (a) Viewing angle change of the plane object image and (b) deformation of the image along depth direction reconstructed by a tilted plane wave incident on the on-axis Fresnel hologram.

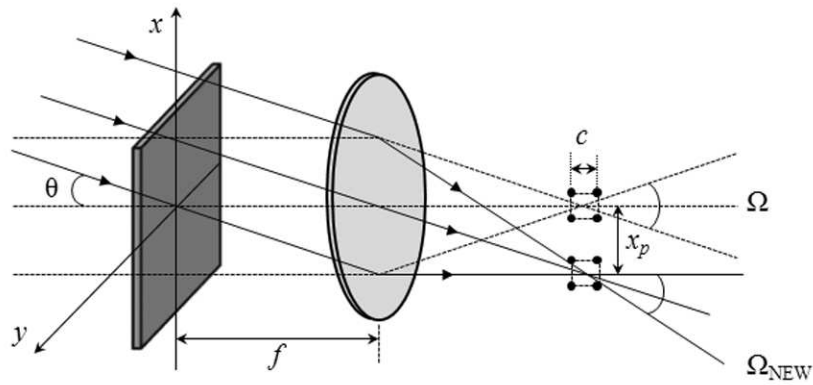


Fig. 3. Viewing angle change of the object image reconstructed by a tilted plane wave incident on the on-axis Fourier hologram.

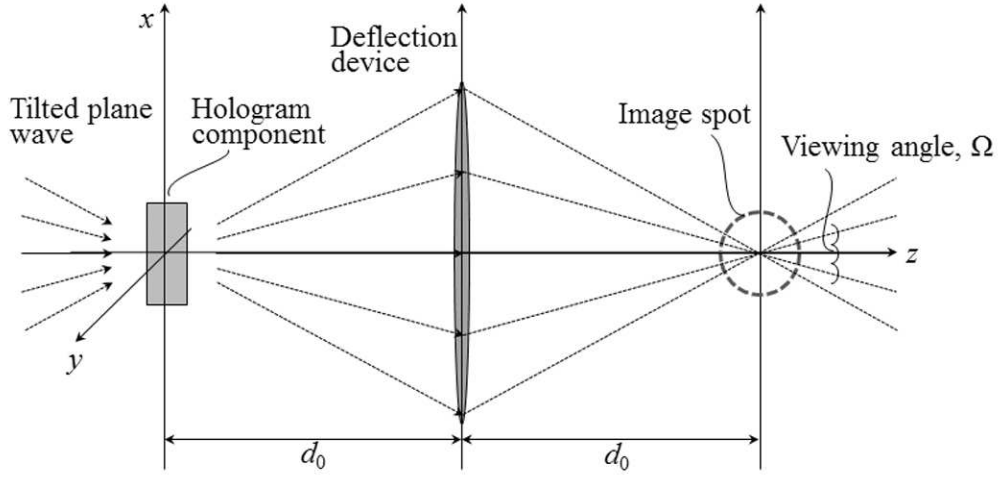


Fig. 4. Typical diagram of obtaining a wide viewing angle of the holographic image by varying an incidence angle of the plane wave.

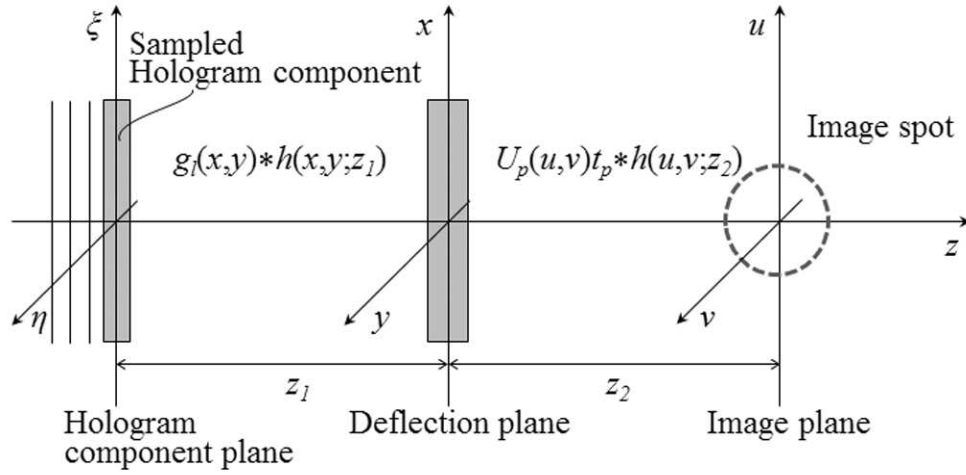


Fig. 5. Schematic diagram of describing the collection of diffraction beams emanated from the sampled hologram.

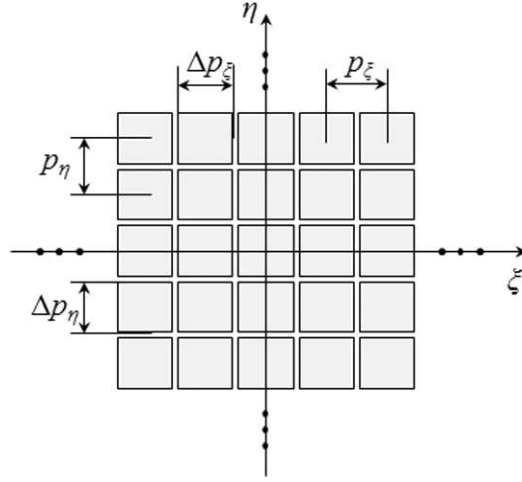


Fig. 6. The pixel structure of the sampled hologram.

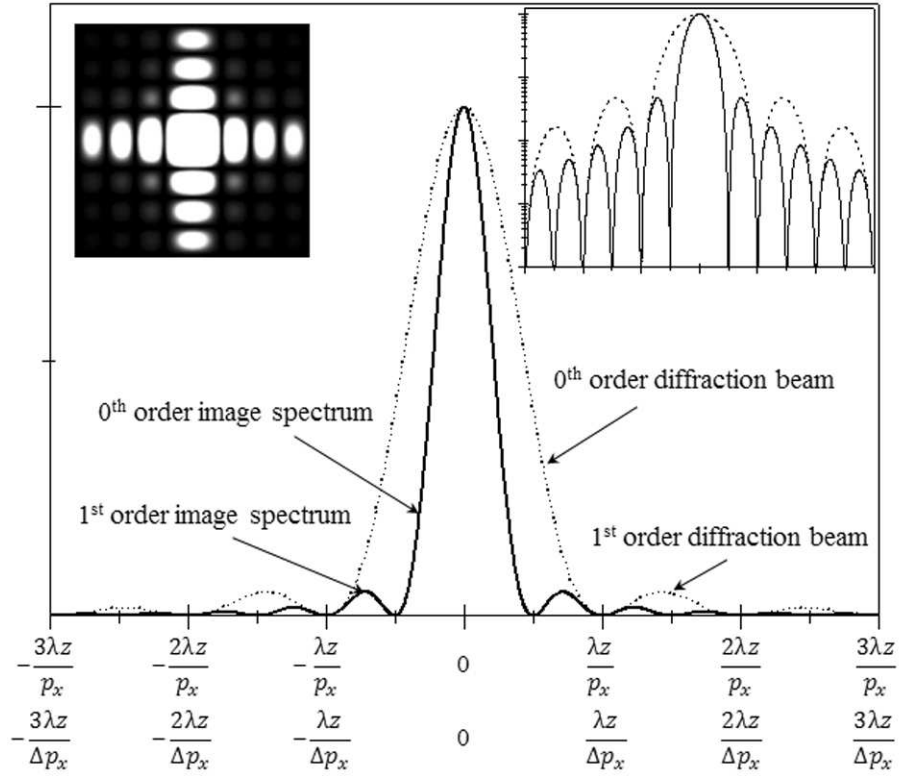


Fig. 7. Modulation of the periodic Fourier spectrum by the envelope of the sinc function along the x -axis. Right inset is the diffraction beam images. Left inset is the resized figure to the logarithmic scale.

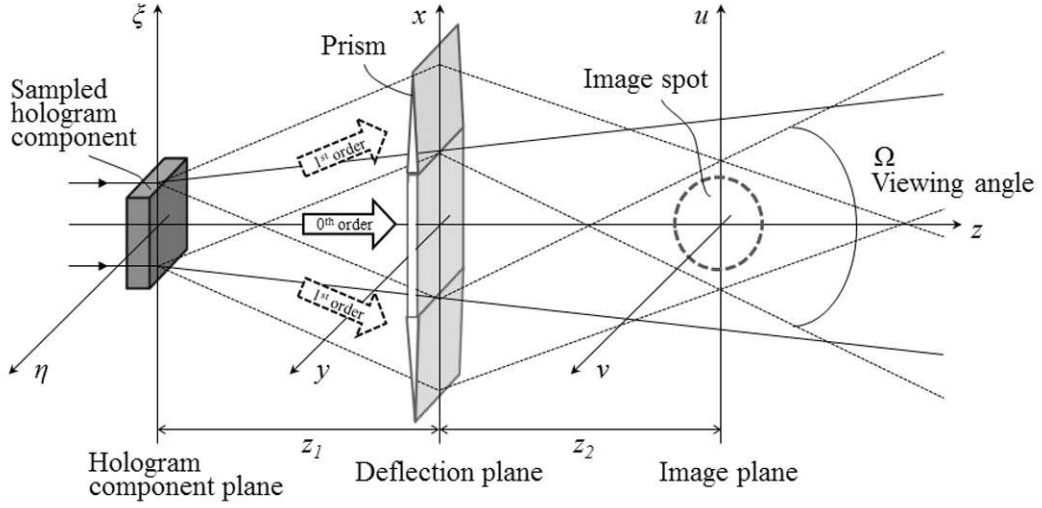


Fig. 8. Illustration of holographic display system for collecting high-order diffraction beams to the image plane by using the optical deflection device.

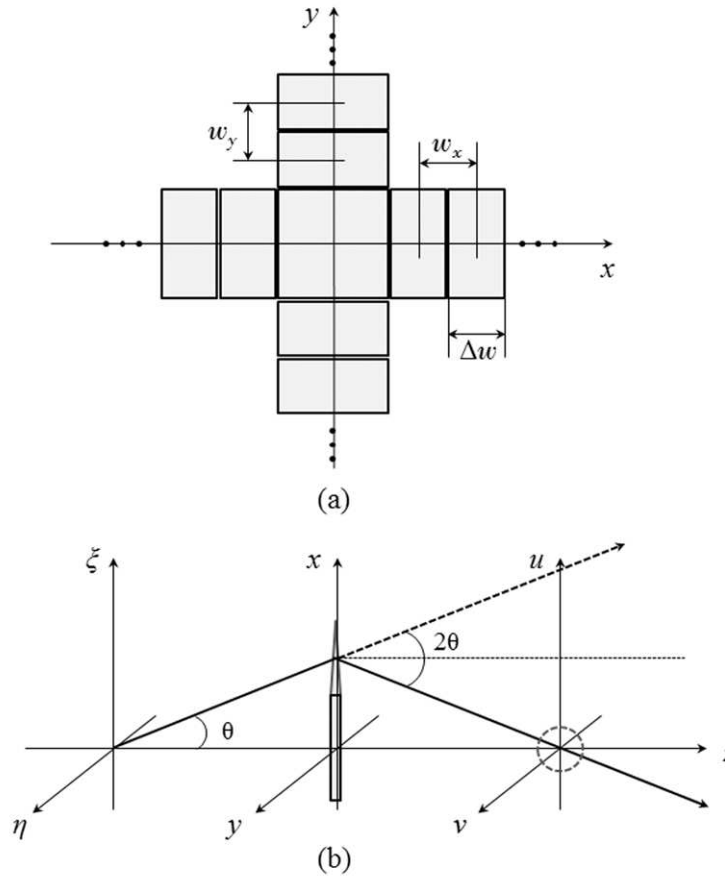


Fig. 9. (a) Alignment of the optical deflection devices and (b) the deflection of diffraction beam.

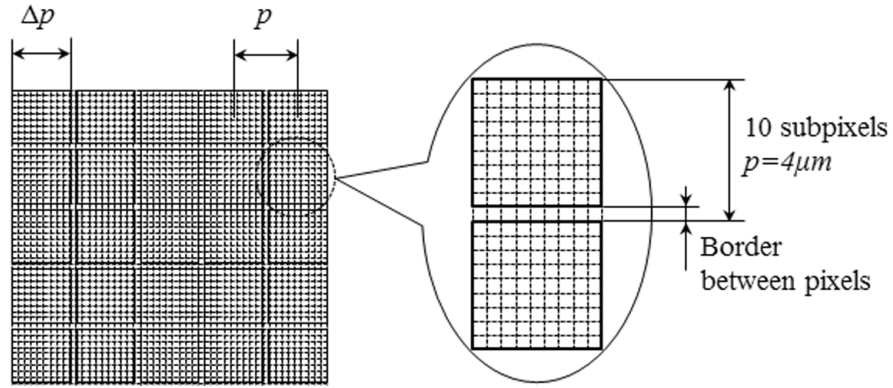


Fig. 10. Outline of the sampled hologram for the numerical analysis.

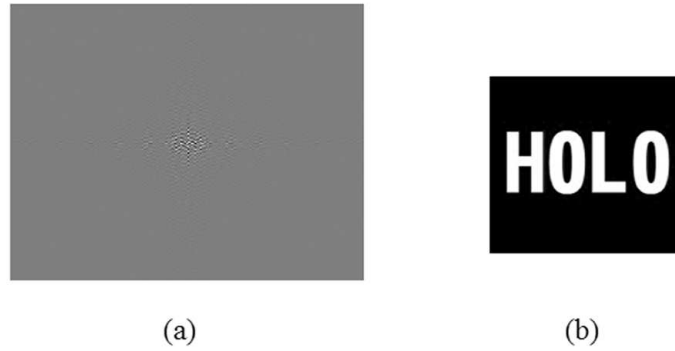


Fig. 11. (a) Sampled hologram with 200×200 resolution prepared from (b) the object of 'HOLO' letter.

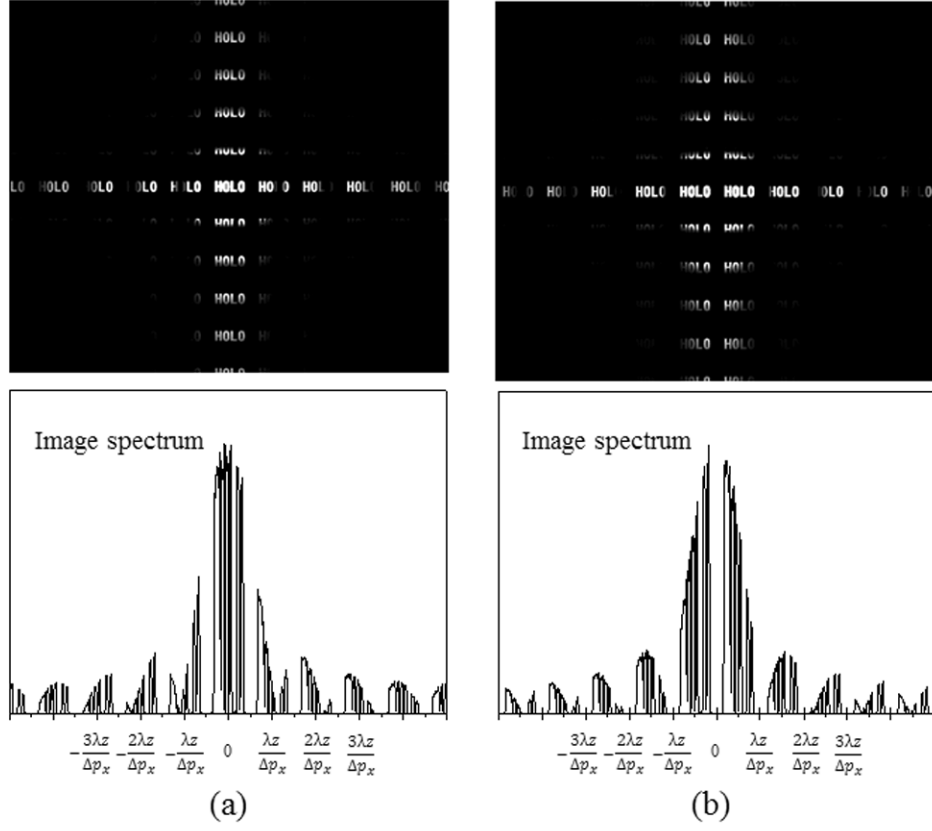
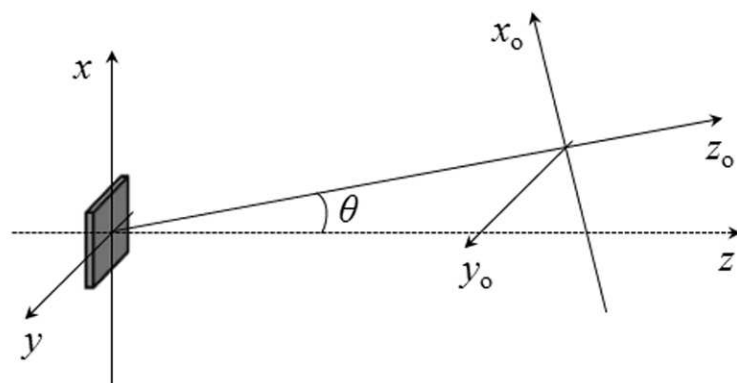


Fig. 12. Numerically reconstructed images and image spectrums for (a) the sampled on-axis hologram and (b) the hologram made by using the phase-shift technology. Central cross-section spectrum along the x -axis is presented.



(a)



(b)

Fig. 13. (a) Geometry of the coordinate transformation to the diffraction direction. (b) The several object views reconstructed at the tilted axis.